Imaging from multiply scattered waves

Romina Gaburro[a], Clifford J. Nolan [a], Thomas Dowling [a]and Margaret Cheney [b]

[a]Dept. of Maths and Statistics, University of Limerick, Castletroy, Ireland;
[b]Dept. of Mathematical Sciences, Rensselaer Polytechnic Institute, Troy, U.S.A.

ABSTRACT

We consider the problem of imaging in a region where ultrasonic waves are multiply scattered. A transducer emits ultrasonic pulses in tissue where they scatter from a heterogeneity (e.g. a tumor) in the region of interest (ROI). The reflected signals are recorded and used to produce an image of tissue. Many of the conventional imaging methods assume the wave has scattered just once (Born-approximation) from the heterogeneity before returning to the sensor to be recorded. In reality, waves can scatter several times before returning to the detector. The purpose of this paper is to show how this restriction (the Born approximation or weak, single-scattering approximation) can be partially removed by incorporating a-priori known environmental scatterers, such as a cavity wall or bones into the background velocity model in the context of acoustic medical imaging. We also show how the partial removal of the Born approximation assumption leads to an enhanced angular resolution of heterogeneities that are present. We will illustrate our method using a locally planar scatterer, which is one of the simplest possible environments for the scatterer.

Keywords: Ultrasonic, Imaging, Multiple Scattering, Backprojection

1. INTRODUCTION

In ultrasonic medical imaging, high-frequency acoustic energy is transmitted into the human body using a set of transducers. The ultrasound waves reflect from boundaries between organs and surrounding fluid, and between regions of differing tissue density. This technique has been used to observe the condition and behavior of fetuses prior to birth. It has also been used to locate tumors, and to observe the condition of the human muscles and bones. Ultrasound inverse scattering is particularly useful for breast cancer screening, because it provides the quantitative sound speed reconstruction of tissue. In practice, large scale ring array acquisition systems are required and the associated hardware becomes very expensive. To solve this problem one can replace the large ring array with a smaller linear one that can be moved along the surface of the tissue in the ROI. We will assume that we are dealing with such a situation in this paper.

Multiply scattered waves are often neglected in imaging methods; largely because of the inability of popular algorithms to deal with the associated non-linear models. This paper shows that by incorporating a known environment (responsible for multiple scattering) into the background model, we can retain both the benefits of imaging techniques based on linear models, as well as obtaining different views of the target scatterer. The net result is an enhanced angular resolution of the target to be imaged.

One of the commonest scattering approximations is the *Born* approximation. This is a single (weak) scattering approximation, which assumes that when a wave is emitted from a source, it only scatterers from the target to be imaged once and then returns to the detector. In reality, waves will scatter several times before returning to the detector. For example, the wave may scatter from other intermediate targets, or it may scatter from an a-priori known scatterer, such as a cavity wall or bones in the context of ultrasonic imaging modality. We propose to incorporate known scatterers, such as a simple perfectly reflective wall, into the background model.

We represent the reflective planar surface using the method of images, incorporate it into the background velocity model, and calculate the corresponding Green's function. From this we develop a modelling operator that maps the oscillatory component of the model (heterogeneities) to the oscillatory component of the scattered wave field that is measured at the transducer. We thus obtain a linear map from model to data, called the

Further author information: (Send correspondence to Romina.Gaburro)
E-mail: Romina.Gaburro@ul.ie, Telephone: 353 61 202700

Medical Imaging 2007: Ultrasonic Imaging and Signal Processing, edited by Stanislav Y. Emelianov, Stephen A. McAleavey, Proc. of SPIE Vol. 6513, 651304, (2007) · 1605-7422/07/$18 · doi: 10.1117/12.712569

scattering operator. The full data set that is collected contains four kinds of scattering events in it, due to the fact that the presence of the wall implies that there are four ways for the wave to scatter on its way from the source to the target and back to the receiver location again (see Figure 1).

We produce an image of the ROI, using a standard backprojection method.[1] This procedure involves applying a weighted adjoint of the scattering operator to the data.

The data that is collected contains all four kinds of scattering events in it. However, by beam forming, it is possible to isolate the individual data from the different experiments. We refer the reader to[2] for a more detailed description of the method and to,[3] where this sort of approach is investigated in the context of known point scatterer in proximity to the ROI. The outline of the paper is as follows. In section 2, we develop a scattering model for scattered waves in the presence of a vertical wall. This is achieved through the use of the method of images. In section 3, we briefly review how to carry out imaging from the data we isolated from experiments 1 and 4 and then very briefly from experiments 2 and 3. In the section 4, we present some numerical simulations to illustrate our ideas and show that method works in the simplest case when the transducer is moved along a series of lines.

2. THE MATHEMATICAL MODEL

2.1. A Model for the Wave Propagation.

We consider the acoustic wave equation

$$\left(\nabla^2 - \frac{1}{c^2(x)}\,\partial_t^2\right)U(t,x) = f, \tag{1}$$

which describes the propagation of the presure $U(x,t)$ sound waves in an inhomogeneous medium with sound speed $c(x)$ and source f.

As in[2] we make the following assumptions

ASSUMPTION 1. We assume that the ROI is well separated from the region where the transducer is located and that in the intervening region, the coefficient in the wave equation (1), is a sum $c(x) + c_0$, where c_0 is known and can be either constant or variable. The coefficient $c(x)$ is an unknown perturbation that we wish to recover from the scattered waves.

ASSUMPTION 2. We assume an environmental scatter near the ROI which is of the form of a vertical wall. From a mathematical perspective, the wall can be taken to be the infinite vertical plane[2] $x_1 = 0$. We assume the ROI lies on one side of this wall.

ASSUMPTION 3. The boundary condition at the wall is the Dirichlet boundary condition

$$U(t,x)|_{x_1=0} = 0. \tag{2}$$

2.2. *Wave propagation in the vicinity of a vertical wall*

The Dirichlet Green's function G with source at y^0 satisfies

$$\begin{cases} \big(\nabla^2 - \frac{1}{c_0^2(x)}\,\partial_t^2\big)G = -\delta(t)\,\delta(x-y^0), \quad \text{for} \quad x_1 > 0 \\ G|_{x_1=0} = 0 \\ G|_{t\ll 0} = 0 \end{cases}$$

with the latter condition ensuring causality.

DEFINITION 2.1. *For any point $x = (x_1, x_2, x_3)$, we denote by $\tilde{x}$ its reflection with respect to the wall, $x_1 = 0$, i.e.*

$$\tilde{x} = (-x_1,\, x_2,\, x_3). \tag{3}$$

By the method of images,[2,4] we can write G explicitly as

$$G(t,\, x - y^0) = \frac{\delta\big(t - \frac{|x-y^0|}{c_0}\big)}{4\pi|x-y^0|} - \frac{\delta\big(t - \frac{|x-\tilde{y}^0|}{c_0}\big)}{4\pi|x-\tilde{y}^0|}, \tag{4}$$

where y^0 and $\widetilde{y^0}$ are the locations of the real and virtual point sources respectively.

2.3. *A linearized scattering model*

Let us denote by V the reflectivity function

$$V(x) = C_0^{-2}(x) - c^{-2}(x) \tag{5}$$

For a sensor located at y the measured signal can be written[2]

$$\begin{aligned}
S(t,y;j_s,j_r) \approx & \int \frac{e^{-i\omega\left(t-2|z-y|/c_0\right)}}{(4\pi)^2 \mid z-y \mid^2}\omega^2 p(\omega) j_s\big(\omega(\widehat{z-y}),y\big) j_r\big(\omega(\widehat{z-y}),y\big)V(z)d\omega dz \\
& - \int \frac{e^{-i\omega\left(t-(|z-y|+|z-\tilde{y}|)/c_0\right)}}{(4\pi)^2 \mid z-y^0 \mid\mid z-\tilde{y} \mid}\omega^2 p(\omega) j_s\big(\omega(\widehat{z-\tilde{y}}),y\big) j_r\big(\omega(\widehat{z-y}),y\big)V(z)d\omega dz \\
& - \int \frac{e^{-i\omega\left(t-(|z-y|+|z-\tilde{y}|)/c_0\right)}}{(4\pi)^2 \mid z-y \mid\mid z-\tilde{y} \mid}\omega^2 p(\omega) j_s\big(\omega(\widehat{z-y}),y\big) j_r\big(\omega(\widehat{z-y}),y\big)V(z)d\omega dz \\
& + \int \frac{e^{-i\omega\left(t-2|z-\tilde{y}|/c_0\right)}}{(4\pi)^2 \mid z-\tilde{y} \mid^2}\omega^2 p(\omega) j_s\big(\omega(\widehat{z-\tilde{y}}),\tilde{y}\big) j_r\big(\omega(\widehat{z-y}),y\big)V(z)d\omega dz.
\end{aligned} \tag{6}$$

where j_s, j_r are weighting functions that summarize the effect of beam forming on transmission and reception respectively.

3. IMAGING

The idealized inverse problem consists in determining V from knowledge of $S(t,y)$ for an interval of time, $t \in [0,T]$ and for y on a given surface parametrised by

$$\Gamma_+ := \big\{\mathbf{\Gamma}_+(s) \;\mid\; s=(s_1,s_2),\; s_1^{min} < s_1 < s_1^{max},\; s_2^{min} < s_2 < s_2^{max}\big\}. \tag{7}$$

We also define

$$\Gamma_- := \big\{\mathbf{\Gamma}_-(s) \;\mid\; s=(s_1,s_2),\; s_1^{min} < s_1 < s_1^{max},\; s_2^{min} < s_2 < s_2^{max}\big\}, \tag{8}$$

which is the mirror image (reflection across the wall) of the curve Γ_+.

To avoid artifacts in the image due to the abrupt edges of Γ_+ and time, we multiply the data by a *mute* $m(s,\, t)$, which is a smooth cutoff function with compact support $supp(m) \subseteq [s_1^{min},\, s_1^{max}] \times [s_2^{min},\, s_2^{max}] \times [0,\, T]$. We denote the *forward map* from scene V to data $d = mS$ by F, so that

$$
\begin{aligned}
F\,V(s,t;j_s,j_r) &= \int e^{-i\omega\left(t-2|z-\Gamma_+(s)|/c_0\right)}\, A_1(z,\ s,\ t,\ \omega;j_s,j_r)\, V(z)\, d\omega\, dz \\
&- \int e^{-i\omega\left(t-(|z-\Gamma_+(s)|+|z-\Gamma_-(s)|)/c_0\right)}\, A_2(z,\ s,\ t,\ \omega;j_s,j_r)\, V(z)\, d\omega\, dz \\
&+ \int e^{-i\omega\left(t-(|z-\Gamma_+(s)|+|z-\Gamma_-(s)|)/c_0\right)}\, A_3(z,\ s,\ t,\ \omega;j_s,j_r)\, V(z)\, d\omega\, dz \\
&+ \int e^{-i\omega\left(t-2|z-\Gamma_-(s)|/c_0\right)}\, A_4(z,\ s,\ t,\ \omega;j_s,j_r)\, V(z)\, d\omega\, dz \\
&:= [F_1+F_2+F_3+F_4]\, V(s,t;j_s,j_r) \qquad (9)
\end{aligned}
$$

where the amplitudes A_j, $j=1,\ldots,4$ include the beam patterns for transmission and reception, the transmitted waveform, the $1/r^2$ geometrical spreading factors and the mute function. We see that the term F_1 corresponds to direct scattering, F_2 corresponds to path 2, etc.

We need to make the following technical assumption[2]

ASSUMPTION 4. *For any $j=1,\ 2,\ 3,\ 4$, the amplitudes A_j satisfy the following supremum (*sup*) estimates*

$$
\sup_{(s,\,t,\,x)\in K} |\ \partial_\omega^{\alpha}\,\partial_s^{\beta}\,\partial_t^{\delta}\,\partial_x^{\rho}\, A_j(x,\ s,\ t,\ \omega)\ | \le C^{j}_{K,\,\alpha,\,\beta,\,\delta,\,\rho}(1+\omega^2)^{(2-|\alpha|)/2}, \qquad (10)
$$

where K is any compact set and α,β,δ,ρ are arbitrary multi-indices of the appropriate dimension.

Assumption 4 is valid for example, when the waveform P is approximately a delta function and the transducer is sufficiently broadband (see[1,5] for further discussion of this). We note that under Assumption 4, the forward operators F_j are so-called Fourier integral operators (FIOs)[6] for $j=1,\ 2,\ 3,\ 4$. Much of the explicit calculation that we show in this paper comes from the abstract underlying properties of FIO's but we do not dwell on such matters here.

3.1. *Image formation from individual data sets*

By choosing the beam patterns $j_s,\ j_r$ appropriately, we can isolate separate data sets

$$
d_i(s,t) = F_i V(s,t),\ \ i=1,2,3,4 \qquad (11)
$$

from the full data set $d=FV$ (see[2] for a more in-depth discussion on this matter).

We apply matched filters (i.e. backproject) with the same phase of the adjoint $F_i^{\star}$ of F_i to the data set d_i in order to reconstruct an image of the scatterers by using separated data (see[2]). The appropriate images $I_i(x)$ at a point x are therefore

$$
\begin{aligned}
I_1(x) &:= \int e^{i\omega\,\left(t-2|x-\Gamma_+(s)|/c_0\right)}\, a_1(x,s,t,\omega)\, d_1(s,\ t)\, d\omega\, ds\, dt, \\
I_2(x) &:= \int e^{i\omega\,\left(t-(|x-\Gamma_+(s)|+|x-\Gamma_+(s)|)/c_0\right)}\, a_2(x,s,t,\omega)\, d_2(s,\ t)\ d\omega\, ds\, dt, \\
I_3(x) &:= \int e^{i\omega\,\left(t-(|x-\Gamma_+(s)|+|x-\Gamma_+(s)|)/c_0\right)}\, a_3(x,s,t,\omega)\, d_3(s,\ t)\, d\omega\, ds\, dt, \\
I_4(x) &:= \int e^{i\omega\,\left(t-2|x-\Gamma_-(s)|/c_0\right)}\, a_4(x,s,t,\omega)\, d_4(s,\ t)\, d\omega\, ds\, dt.
\end{aligned}
$$

where the amplitudes $a_i,\ i=1,2,3,4$ are to be chosen later.

We will only explicitly deal with the image I_1 because this case is the simplest one and has already been investigated.[1,2] We will briefly review the analysis of this image because it gives a flavor of how the analysis of

the remaining images proceeds. Indeed, the analysis of image I_4 is identical to that of I_1 because we need only change the location of the source to the virtual source. For images I_2 and I_3, we can refer to the geophysics literature that involves common mid-point geometry.[7] We can also refer to[5] for an even more explicit analysis. Even though we are dealing with this kind of special geometry, our data set is very rich - we have what we refer to as a full data set. In[5,7] it was shown that except in very exceptional cases, backprojection succeeds. The analysis is not as explicit as that for image I_1 below but it is similar in spirit. Let us proceed by analyzing the image I_1:

$$I_1(x) \ = \int e^{i\phi_1(s,t,x,z,\omega,\tilde{\omega})}\, b_1(s,t,x,z,\omega,\tilde{\omega})\, V(z)\, dz\, d\omega\, d\tilde{\omega}\, dx\, ds\, dt \tag{12}$$

where

$$\phi_1(s,x,z,\omega) = 2\omega\big(\ |\ z-\Gamma_+(s)\ |\ \ -\ |\ x-\Gamma_+(s)\ |\ \big)/c_0 \tag{13}$$

$$b_1(s,x,z,\omega) = a_1(x,s,2|x-\Gamma_+(s)|/c_0,\omega)A_1(z,s,2|x-\Gamma_+(s)|/c_0,\omega) \tag{14}$$

after performing a stationary phase calculation[2] in the variables $(\tilde{\omega},t)$. Therefore

$$\phi_1(s,x,z,\omega) = f_1(z,s,\omega) - f_1(x,s,\omega) \tag{15}$$

where

$$f_1(z,s,\omega) = 2\omega|z-\Gamma_+(s)|/c_0 \tag{16}$$

Using Taylor's theorem, we obtain

$$\begin{aligned} \phi_1(s,x,z,\omega) &= (x-z)\cdot\Xi(z,x,s,\omega) \\ \Xi(z,x,s,\omega) &:= -\int_0^1 \nabla_z f_1((1-\lambda)x+\lambda z,s,\omega)\ d\lambda \end{aligned} \tag{17}$$

Consequently,

$$I_1(x) = \int e^{i(x-z)\cdot\Xi(z,x,s,\omega)}\ b_1(s,x,z,\omega)V(z)\ dzd\omega ds \tag{18}$$

Remark 1. By a stationary phase argument, we can assume without loss of generality that the amplitude b_1 need only be non-zero near $z=x$. Indeed, the error made by violating this assumption is an integral whose integrand is rapidly decaying in ω and hence infinitely smooth. We are willing to ignore such errors in our approximation, instead concentrating on recovery of (high-frequency) singularities in V.

Let us consider the map

$$\psi_1 : (s,\omega) \mapsto \Xi(x,x,s,\omega) := -2\omega/c_0\ \left(\widehat{R_x^+}\right)_H \tag{19}$$

where

$$R_x^+ = x-\Gamma_+(s) \tag{20}$$

and the subscript H stands for the horizontal component (first two components). For z,x fixed, we observe[1,2] that the map

$$(s,\omega) \mapsto \Xi(z,x,s,\omega)$$

is a diffeomorphism near $z=x$, provided that x is not directly beneath the transducer location $\Gamma_+(s)$.

After the change of variable, we obtain

$$I_1(x) \approx \int e^{i(x-z)\cdot\xi}\ \tilde{b}_1(x,z,\xi)V(z)\ dzd\omega ds \tag{21}$$

where $\tilde{b}_1$ incorporates that Jacobian factor from the change of variable. It is possible to choose the original amplitude a_1 so that $\tilde{b}_1$ is equal to $(2\pi)^{-n}$ for those values of (z, ξ) belonging to a certain open set. Then, (21) looks like a filtered Fourier inversion of the Fourier transform of V. The only thing missing is that not all Fourier directions ξ are present. Further interpretation to the reconstructed image can be given by considering the notion of *wavefront set*[2,8] of V. Therefore we have shown that the reconstruction I_1 is approximately the Fourier inversion over as large a solid angle for the frequencies as possible.

The imaging analysis of I_2 and I_3 is identical to that of I_1, up to (19), with f_1 now being replaced by

$$f_1(z, s, \omega) = \omega(|z - \Gamma_-(s)| + |z - \Gamma_+(s)|)/c_0 \tag{22}$$

and (19) replaced by

$$\Xi(x, x, s, \omega) = -\omega/c_0 \ \left(\widehat{R_x^+} + \widehat{R_x^-}\right)_H \tag{23}$$

where

$$R_x^- = x - \Gamma_-(s). \tag{24}$$

We have seen from (19) that for a fixed x, the map

$$\psi_1 : (s, \omega) \to -\omega/c_0 \left(\widehat{R_x^+}\right)_H \tag{25}$$

is a local diffeomorphism (we omit the factor 2 for what comes next). Let

$$-\omega/c_0 \ \left(\widehat{R_x^+}\right)_H = (l, m) \tag{26}$$

so that the map

$$(s, \omega) \to (l, m) \tag{27}$$

is a local diffeomorphism.

It is not difficult to deduce that

$$\psi_2 : (s, \omega) \to -\omega/c_0 \left(\widehat{R_x^+} + \widehat{R_x^-}\right)_H \tag{28}$$

is also a local diffeomorphism.[2]

Therefore we have shown that the backprojection algorithm works in the multiple scattering situtation, provided we separate out the various data signals corresponding to the paths 1 through 4 and form the corresponding images I_1 through I_4.

4. NUMERICAL EXPERIMENTS

To validate our theory that the backprojection works with improved performance using mulitply scattered waves, we did the following set of experiments. A simple 'bump' reflectivity function V was positioned with co-ordinates $(50, 50)$ in a 100×100 grid, as shown in figure (2). The reflectivity function was confined to a thin layer located at a distance 8 units (cm) from the surface of the tissue (skin), which we assume to be horizontally flat in these experiments. Figure (2) shows this cross section. The environmental scatter (known) is located at zero horizontal units (i.e., the Y-axis).

A typical acquisition track along which we acquired the data was a straight line track, and the data associated to paths 1 to 4 in figure (1) are all present in figure (3). Note that paths 2 and 3 are the same length and so the signals for these paths are superimposed on one another.

Figure (4) shows the backprojected image obtained from a single acquisition track, containing the scattering data from path 1 in figure (1) only. It contains a well known artifact that is symmetrically placed with respect to the track. When we include the scattering data from all of the paths 1 to 4 in figure (1), we see an improved image in figure (5), with a suppression of the former artifact.

Figures (6,7) show the corresponding images including all acquisition tracks, using direct scattering data (path 1) and all of the scattering paths (paths 1 to 4) respectively. The range extent of these tracks is detailed in the captions to these figures. Clearly, incorporating the multiply scattered waves into our imaging algorithm has improved it - the different views of the bump function are clearly visible when we include this kind of data.

5. CONCLUSIONS

This paper is a step forward in including multiple scattering in imaging methods. It shows that by incorporating a known environment into the background model, we can retain both the benefits of imaging techniques based on linear models, as well as obtaining different views of the ROI. The net result is an enhanced angular resolution of the target to be imaged. Finally, we hope to improve the method to the point where it is no longer necessary to know the environmental scatter a-priori but instead estimate it simultaneously along with the ROI.

ACKNOWLEDGMENTS

TD, RG and CN acknowledge the support of Science Foundation Ireland (Grant 03/IN3/I401). MC acknowledges the support of IPAM and AFOSR (grant FA9550-06-1-0017).

REFERENCES

1. C. Nolan and M. Cheney, "Synthetic aperture inversion for arbitrary flight paths and non-flat topography," *IEEE Trans. on Image Processing* **12**, pp. 1035–1043, 2003.
2. T. D. C. Nolan, M. Cheney and R. Gaburro, "Enhanced angular resolution from multiply scattered waves," *Inverse Problems* **22**, pp. 1817–1834, 2006.
3. M. Cheney and R. Bonneau, "Imaging that exploits multipath scattering from point scatterers," *Inverse Problems* **20**, pp. 1691–1711, 2004.
4. P. M. . H. Feshbach, *Methods of Theoretical Physics, Vol. 1*, McGraw-Hill, 1953.
5. M. C. C. Nolan, "Synthetic aperture inversion," *Inverse Problems* **18**, pp. 221–236, 2002.
6. J. Duistermaat, *Fourier Integral Operators*, Birkhauser, Boston, 1996.
7. C. J. Nolan and W. W. Symes, "Global solution of a linearized inverse problem for the wave equation," *Comm. in PDE* **Vol 22(5&6)**, pp. 919–952, 1997.
8. X. S. Raymond, *Elementary Introduction to the Theory of Pseudodifferential Operators*, CRC Press, 1991.

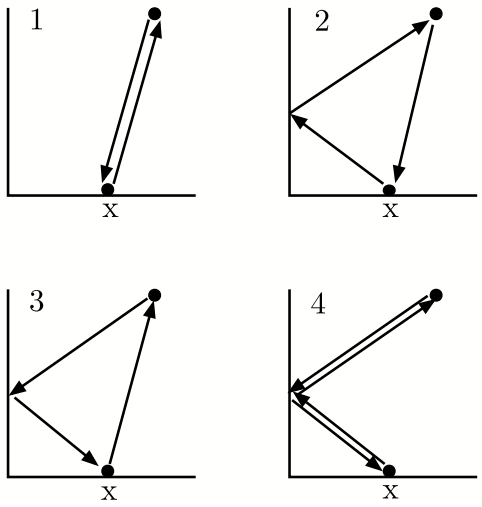

Figure 1. In path 1, the wave scatters directly to and from the heterogeneity ($\mathbf{x}$). In path 2, the wave scatters from the wall to $\mathbf{x}$ and back to the receiver. In path 3, the wave scatters from $\mathbf{x}$ to the wall and back to the receiver. Finally, in path 4, the wave scatters to the wall to $\mathbf{x}$ and back to the wall again before returning to the receiver.

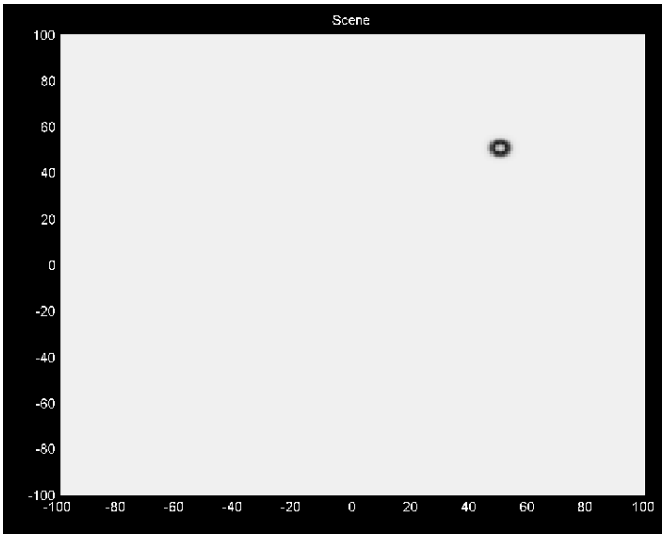

Figure 2. Model reflectivity function to be reconstructed. It is a simple 'bump' function with its center located at $(50, 50)$.

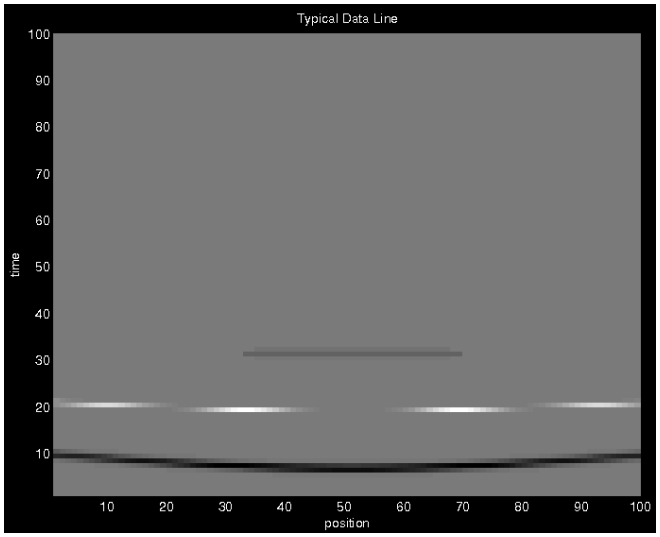

Figure 3. This is how a typical data record looks like for a single acquisition track along which the sensor travels. In this case, the track is located along a line with horizontal coordinates 65 and vertical range running from 25 to 75.

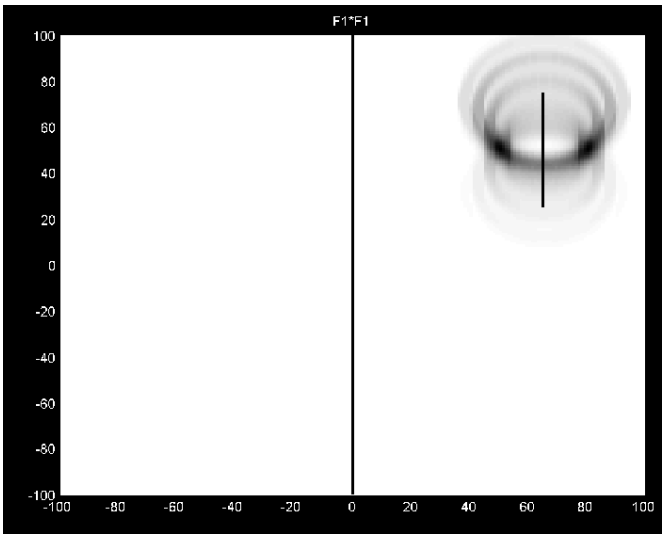

Figure 4. Here we show how a typical image looks like from a single track acquisition, where we just use the directly scattered signal, i.e., this figures represents a typical I_1.

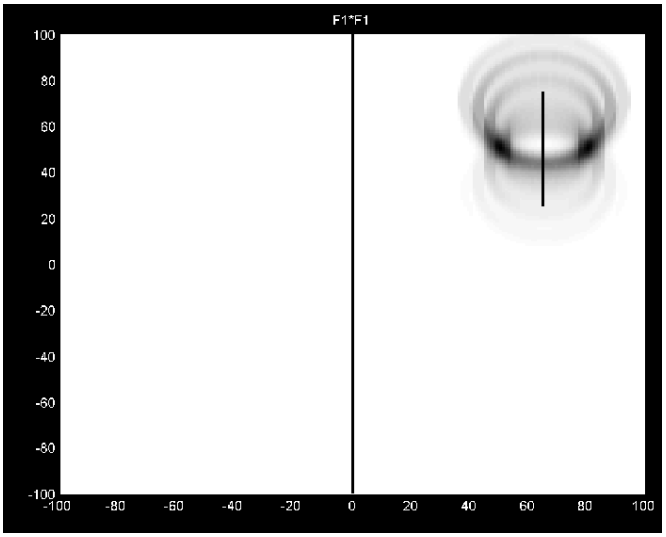

Figure 5. Here we show how a typical image looks like from a single track acquisition, where we just use the multiply signals, i.e., this figures represents a typical I_2 or I_3.

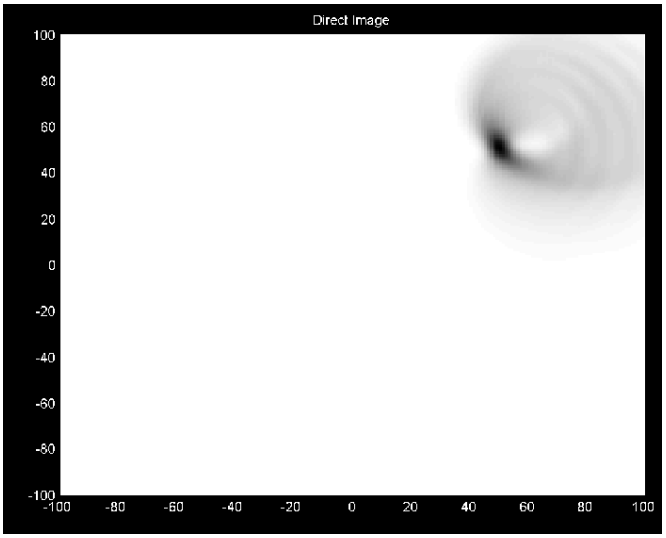

Figure 6. This is the total image obtained from combining the information in vertical tracks with horizontal range from 60 to 80 and vertical range 25 to 75. Only the directly scattered signal corresponding to path 1 is used here.

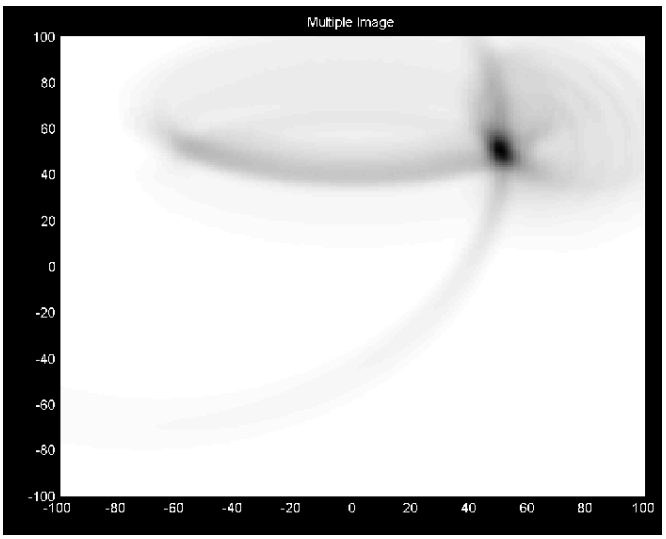

Figure 7. This is the total image obtained from combining the information in vertical tracks with horizontal range from 60 to 80 and vertical range 25 to 75. All scattering paths are used to obtain the combined image here, providing an improved angular resolution of the original model.